SSRG International Journal of Mechanical Engineering
ISSN: 2348-8360/ https://doi.org/10.14445/23488360/IJME-V13I7P105

Volume 13 Issue 7, 57-68, July 2026
© 2026 Seventh Sense Research Group®

Original Article

Modelling and Performance Analysis of a Combined SOFC-GT System with HRSG

Amit Talukdar[1], Pranjal Sarmah[1*], Partha Protim Borthakur[1]

[1]*Mechanical Engineering Department, Dibrugarh University, Dibrugarh, Assam, India.*

[*]*Corresponding Author : pksnit07@dibru.ac.in*

Received: 06 March 2026 Revised: 30 April 2026 Accepted: 01 July 2026 Published: 30 July 2026

Abstract *- This paper presents an energy and exergy analysis of a Solid Oxide Fuel Cell (SOFC)-Gas Turbine (GT) configuration integrated with a Heat-Recovery Steam Generator (HRSG) to generate steam for industrial use. The simulation of the hybrid powerplant was performed over a Compression Pressure Ratio (CPR) range of 8-16, with variations in air and fuel supply. The net power output, along with energy and exergy efficiencies, increases with increasing CPR. Without additional fuel supply to the combustion chamber, the total power output of the system is 40.92 MW, with energy and exergy efficiencies are 61.23% and 59.15%, respectively, at CPR 16. The net power output with additional fuel input (50-150 kmol/hr) increases to 50 MW at 150 kmol/hr, at 16 CPR; however, the thermodynamic efficiency decreases owing to increasing Irreversibility. The component-level irreversibility analysis indicates maximum exergy destruction at the SOFC, followed by the CC. The steam generated within the HRSG by utilising the GT exhaust stream increases with additional fuel, reaching 12.27 kg/sec at 16 CPR. The study highlighted the trade-off between efficiency improvement and net power enhancement in the proposed configuration.*

Keywords *- Solid Oxide Fuel Cell, Gas Turbine, Energy and Exergy Analysis, Hybrid Power System, Compression Pressure Ratio.*

1. Introduction

Climate change is now a more serious and challenging concern for countries than ever before. The year 2024 was the warmest on record, and the period from 2015 to 2024 was the hottest on record [1]. According to the IEA, energy-related emissions are rising. Although electricity accounts for 40 per cent of global energy, the rate of efficiency improvement is well below the targeted 4 per cent [2]. The report further stated that 40 per cent of the energy sector's emissions originate from power-generating plants and that a net-zero-emission scenario requires clean electricity generation technologies.

Fossil fuel-powered thermal power plants deliver two-thirds of the global electricity, with 55–70 per cent of the input energy rejected as waste heat [3]. Conventional power plants, such as steam- and gas-turbine-based plants that rely on fossil fuels, generate substantial electricity; despite their high emissions, they remain in operation. Also, power plant efficiency depends on the technology and the fuel utilised [4]. Governments worldwide are promoting hydrogen-based clean energy sources and renewable energy. Consequently, advanced technologies such as fuel cells are attracting research interest. Among various types of fuel cell technology being investigated, the SOFC is the most versatile due to its ability to operate at high temperatures (650–1000°C), making it less susceptible to carbon poisoning, producing minimal emissions, operating silently, achieving high energy conversion efficiency, and offering fuel flexibility. These properties of SOFCs make them suitable for stationary power generation. On the other hand, gas turbines, first developed in Switzerland in 1939, are limited by the Carnot efficiency [5].

In contrast, SOFC directly convert the chemical energy of a fuel into electricity without combustion. Because SOFC exhaust is high-grade energy, it is imperative to add a bottoming cycle to recover waste heat. Gas turbine and steam turbine power plants can serve as bottoming cycles. The efficiency of gas turbine-based power-generating units ranges from 29–45%, and the electrical efficiency of SOFCs is 45–55% [6]. However, the combined SOFC-GT efficiency exceeds 60 per cent and can attain electric efficiency higher than that of conventional combustion-based systems [7, 8]. The integration of a gas turbine also reduces the size and cost of the SOFC [9].

However, the efficiencies of SOFC-GT vary widely due to differing modelling assumptions, making comparisons difficult [10]. Comprehensive literature reviews by He et al. indicate that the electrical efficiencies of pressurised SOFC GT combined systems range from 52% to 68%, and that efficiency is independent of hybrid system output capacity [11]. The fuel for SOFC power plants is hydrogen supplied

This is an open access article under the CC BY-NC-ND license (http://creativecommons.org/licenses/by-nc-nd/4.0/)

primarily from natural gas and from other sources such as biomass, ammonia, and syngas. However, reforming reactions are essential for extracting hydrogen from hydrocarbon fuels. Internal reforming, external reforming and partial reforming are three types of hydrocarbon reforming procedures [12].

For hydrogen generation, if methane fuel and steam are introduced into the SOFC, the process is internal reforming; if they are introduced into the external prereformer section, the process is external reforming. If a portion of the hydrocarbon is reformed externally and the remainder is reformed within the SOFC, this constitutes partial reforming. The study of fuel cells is primarily conducted using numerical methods, as they are less costly than experimental methods [13].

A unit cell of an SOFC comprises 3 components: a cathode, an anode, and an electrolyte sandwiched between the cathode and anode (Figure 1). The hydrogen fuel fed into the porous anode (fuel electrode) diffuses through it. It reacts with oxygen ions transported across the electrolyte at the triple-phase boundary between the anode and electrolyte [14]. In this oxidation reaction, hydrogen reacts with oxygen ions to produce steam and electrons.

The electron travels via the external electric circuit to the cathode, thereby generating DC. The oxygen supplied to the cathode reacts with electrons at the cathode-electrolyte interface to form the oxygen ion. Concentration gradients and potential differences drive the transfer of oxygen ions through the electrolyte, which acts as an ionic conductor. The following equations (1) and (2) are the electrochemical reactions occurring at the electrodes.

$$\frac{1}{2}O_2 + 2e^- = O^{2-} \quad (1)$$

$$H_2 + O^{2-} = H_2O + 2e^- \quad (2)$$

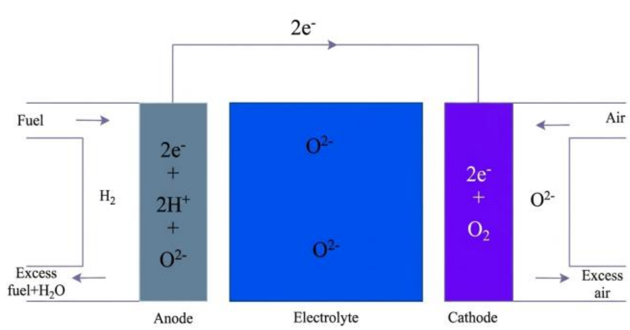

Fig. 1 Principle of SOFC

Material properties are significant because desirable properties can reduce losses, increase efficiency, and improve durability. Table 1 lists the desirable properties of SOFC components. Several unit cells must be connected via an interconnect to generate sufficient DC at high voltage for practical purposes [15].

Table 1. Desirable properties of SOFC material [15, 16]

Conductivity	Electrolytes should exhibit higher ionic or proton conductivity but lower electronic conductivity.
Mechanical strength	Electrolytes should be sufficiently strong to withstand high stress.
Thermal stability & compatibility	Improved thermal stability enables all three components to operate at high temperatures while maintaining thermal compatibility.
Cost effectiveness	Materials must be cost-effective to ensure the economic feasibility of power generation.

Although not as efficient as SOFC, natural gas-powered turbines still have low carbon emissions and low cost [17]. Moreover, the power-to-weight ratio is impressive, and durability is enhanced by the use of rotational parts and low maintenance, with no coolant such as water [18]. ST plants require hours to reach full-load conditions in gas turbines, whereas the GT takes minutes. Given these essential characteristics, several SOFC GT combined systems have been investigated numerically, with only a few companies, such as Mitsubishi and Siemens Westinghouse, developing working prototypes. In 2007, Mitsubishi Heavy Industries demonstrated the working of a 200 kW-class SOFC-MGT plant. The SOFC and the MGT received fuel heat inputs of 339.8 kWh and 51.5 kWh, respectively, and the gross AC power output was 211.1 kW, with a thermal efficiency of 52.1% [19]. Siemens Westinghouse tested a 220 kW SOFC-MGT combined system operating at 3 atm. The SOFC produced 180 kW(e), the GT produced 40 kW(e), and the integrated unit achieved an electrical conversion efficiency of 53% [20].

The literature has focused on the thermodynamic analysis of SOFC-GT power plants, mostly using software such as MATLAB, Aspen Plus, and Cycle Tempo. The size of the SOFC-GT combined systems can range from the kW to the MW scale. Adding more unit cells and stacks to an SOFC can enhance its power output, while integrating it with a GT of suitable capacity further increases the hybrid system's power output. Song et al. studied a possible configuration of a 4.6 MW commercially available turbine integrated with an MW-scale SOFC, using a computational model. The predicted efficiency under pressurised conditions, limited by the fuel cell stack temperature, reaches 58.62% for a power output of 11.5 MW. Cavalli et al. modelled a biomass gasifier SOFC integrated with a micro gas turbine and tested it to increase efficiency using two internal reforming methods [22]. One method, i.e., the afterburner off-gas efficiency, improves electrical efficiency and is therefore recommended for application. In comparison, the other catalytic partial oxidation method, although it improves overall efficiency, is not advised as it reduces electrical efficiency. Wu et al. designed a compressed-fuel unit to simulate the SOFC-GT process in

MATLAB and Aspen Plus, achieving CO_2 emissions of 324.2 g/kWh and hybrid power efficiency of up to 50% [23]. A natural-gas-fed SOFC-GT plant with an additional power turbine configuration was simulated in MATLAB by Chan et al., who studied the effects of pressure and fuel flow [24]. The pressurised system setup, which delivers fuel and air in a compressed state, achieved electrical and overall system efficiencies of 60% and 80%, respectively. In their next research, the same authors simulated a 1.3 MW SOFC hybrid system with an HRSG that generated steam from GT exhaust. The electrical and overall efficiencies exceeded 60% and 80%, respectively [25]. Tarroja et al. investigated variations in several parameters, including pressure ratio, fuel and air utilisation, and current density, for the SOFC-GT plan [26]. The configuration operating under moderate pressure, with air preheated through a heat exchanger and high fuel utilisation with low oxygen utilisation, demonstrated the highest efficiency. The impact of variations in fuel gas composition, controlled by pressure and the fuel utilisation factor, on an SOFC-GT was studied by Corigliano et al. [27]. The overall electrical efficiency ranged from 53% to 63%, with primary energy savings ranging from 33% to 52%. Most of the cited literature reports performance improvements when GT is integrated as a bottoming cycle with an SOFC, compared with a standalone SOFC and GT plant. This is due to the gas turbine utilising the high-grade exhaust heat from the SOFC. The combined systems operating at above-atmospheric pressure demonstrated improved electrical efficiency [21, 24, 26]. Consequently, the cost per MWh for a pressurised system is lower than that for an atmospheric system, making the former economically viable [28]. Similar studies have demonstrated that the thermodynamic efficiency of pressurised SOFC-GT systems exceeds 60% [29]. However, high material and manufacturing costs, advanced control systems, and reliability and durability issues stemming from high SOFC stack temperatures remain key challenges [30].

Limited studies have focused on integrating an HRSG for steam generation into a pressurised SOFC-GT system at the MW scale. The US Department of Energy reported that the pulp and paper industry, petroleum refineries, and chemical manufacturing, which are considered among the Industries Of The Future (IOF), require steam for their operation. In these industries, steam is generated at pressures ranging from 21.7 to 69.9 bar, with boiler steam capacities of 1.1 to 27.4 kg/s [31]. The catalogue of CHP technologies prepared by the US Environmental Protection Agency listed GT systems generating steam in the range of 2.48 kg/sec to 17.39 kg/sec [32]. It highlighted the on-site steam requirement for industrial processes, such as those in the chemical, paper, and petroleum refining industries. Johnson and Fiss demonstrated the generation of superheated steam at temperatures and pressures of at least 300°C and 25 bar from a latent-heat storage system integrated with a cogeneration power plant for industrial purposes [33]. Gogoi et al. conducted a MATLAB simulation of a combined SOFC-GT-ST power plant configuration, demonstrating that additional fuel burning at higher CPR improves plant performance [34]. However, the contribution of a steam turbine to the net power output is comparatively low, and, moreover, the steam turbine's power output decreases as CPR increases, in sharp contrast to the increases in power output from the SOFC and GT units.

Moreover, these systems must be designed based on the hybrid system's power output requirements, fuel type, heat recovery, and operating temperature [30]. Although several SOFC-GT systems with waste-heat recovery systems for steam generation have been studied, limited attention has been paid to a systematic assessment of the simultaneous generation of electricity and superheated steam under various operating conditions. Accordingly, this simulation-based study investigates the performance of the proposed SOFC-GT configuration with an HRSG at different compression pressure ratios, by varying the air-fuel ratio and the additional fuel supplied to the CC. Such a system has the potential to meet IOF's steam requirements while simultaneously generating power for industrial and residential consumption.

2. Configuration Design

The SOFC-GT hybrid plant, as shown in Figure 2, uses a methane-fueled SOFC with a prereformer, air and fuel compressors, fuel and air recuperators, a combustion chamber, a gas turbine and HRSG. The air and fuel at ambient state are compressed to the selected system pressure. The power consumed by air and fuel compressors is deducted from the gas turbine output to obtain the net system power output. Both the air and the fuel are preheated in heat exchangers before being fed to the SOFC. The compressed methane is heated in a fuel recuperator by exchanging heat with the gas turbine exhaust, then sent to the pre-reformer unit. 30 per cent of the fuel is externally reformed in the prereformer unit using steam extracted from the HRSG unit.

The remaining gas is sent to the fuel electrode (anode) for internal reforming. The compressed air for the SOFC cathode is preheated in an air recuperator, while the gas turbine exhaust passes through a fuel recuperator. DC current produced by the SOFC is converted to AC by an inverter. The products of the electrochemical reaction within the SOFC are fed into the Combustion Chamber (CC). The CC includes a provision for additional fuel intake via a fuel line that diverts a portion of the compressed fuel from the fuel compressor. The high-pressure gas generated inside the CC is fed into the GT, where it expands and performs mechanical work, generating AC. The exhaust from GT via AR and FR is channelled to the HRSG for steam generation.

The simulation study in the proposed model considers four air-fuel operating conditions. For each operating case, the pressure ratio is varied from 8 to 16 in increments of 2, with the key parameters listed in Table 2 held constant.

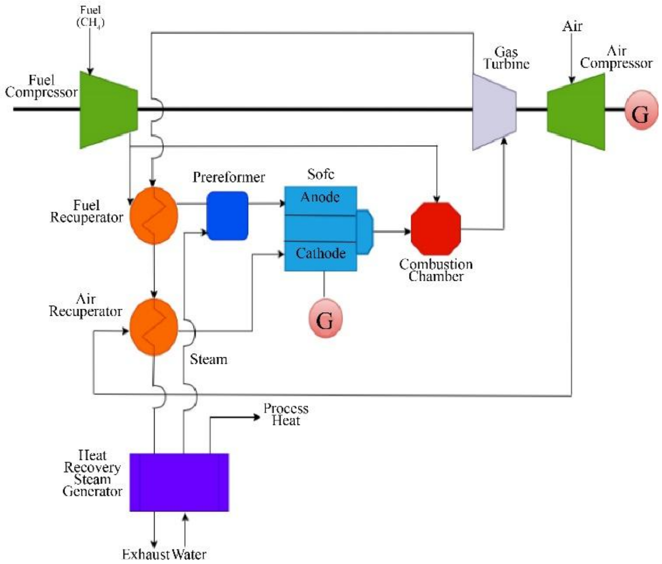

Fig. 2 Schematic of the SOFC-GT plant

MATLAB is used to develop and execute the simulation code, which executes an iterative procedure to compute solutions for several plant-component operations. For every compression pressure ratio and air-fuel combination, power requirements and Irreversibility associated with the compressors are calculated. An initial estimate of the SOFC stack temperature is assumed. The methane reforming and water gas shift equilibrium constants are evaluated. The composition of the SOFC exhaust stream is determined by a specified fuel utilisation factor. The estimated SOFC exhaust is fed to CC and, consequently, to GT. The exhaust stream from GT is routed through the fuel and air recuperator to the HRSG, where the steam generation rate is finally calculated. The prereformer model is supplied with fuel recuperator outlet temperature and a prescribed superheated steam state at a fixed steam-to-carbon ratio. Since the temperatures at the outlet of the SOFC, the prereformer, the recuperators, and the turbine exhaust are iteratively coupled, an iterative calculation was applied. The stack temperature was updated until the relative error between successive estimates was below 10^{-4} with a maximum of 400 iterations. The calculations for the SOFC and prereformer converged with a relative tolerance of 0.005, whereas the internal reforming calculation converged with a relative tolerance of 0.001. Polynomial correlations based on temperature were used to evaluate the enthalpy, entropy, and specific heat of the gases considered

3. Thermodynamic Modelling of the combined System

SOFC-GT systems broadly comprise the following components: SOFC, GT, compressors, pre-reformer unit, combustion chamber, HRSG, and recuperators. Energy and exergy analyses are conducted based on the first and second laws of thermodynamics, respectively. Exergy analysis quantifies the actual efficiency of a system, and the components in which exergy is destroyed represent Irreversibility. The physical, chemical, potential, and kinetic exergies of a system collectively constitute the system's total exergy.

3.1. Assumptions

In thermodynamic modelling, several assumptions adopted by previous studies on SOFC-GT hybrid systems are employed in this simulation-based analysis of the hybrid plant. For the proposed system analysis, the reference environmental pressure and temperature for the dead state are set to 1 atm and 25 °C, respectively. The potential exergy and kinetic exergy have been neglected. For incoming air, both physical and chemical exergy are negligible; for fuel, only the physical exergy is neglected. The gases behave as ideal gases at the electrode and in the CC. The entire process is occurring at a steady state with no leakages. No pressure drop occurs at the HRSG. 100 per cent of the reactants are oxidised during combustion in the CC.

3.2. Equations

3.2.1. SOFC Modelling

The SOFC is modelled considering all cells as identical. The Nernst equation, when the partial pressures of H_2 and O_2 as reactants, and of H_2O as the product, are known, is

$$E_{rev} = \frac{-\Delta G^o}{2F} + \frac{RT}{2F} ln \frac{P_{H_2} P_{O_2}^{1/2}}{P_{H_2O}}$$

Where E_{rev} is the reversible voltage, ΔG^o is the standard Gibbs free energy change of reaction, F is the Faraday constant, R is the universal gas constant, and T is the SOFC operating temperature.

However, Irreversibility reduces the reversible open-circuit voltage. Three types of losses: ohmic (η_{Ohm}), concentration (η_{Conc}), and activation losses η_{Act}, as described below

$$\eta_{Ohm} = i \sum_j \frac{A_j \, exp^{\frac{B_j}{T}} \, \delta_j}{A_{s,j}}$$

where i is the current density, A_j is the preexponential coefficient, B_j is the activation energy parameter, δ_j is the thickness of the layer, $A_{s,j}$ is the active surface area of the layer.

$$i = i_o \left\{ \exp\left(\beta \frac{F\eta_{Act}}{RT}\right) - \exp\left(-(1-\beta)\frac{F\eta_{Act}}{RT}\right) \right\}$$

where i_o is the exchange current density, coefficient, β transfer coefficient

$$\eta_{Conc} = \frac{RT}{nF} \ln\left(1 - \frac{i}{i_L}\right)$$

Considering these three losses, the actual cell voltage is calculated.

$$V = E_{rev} - \eta_{Act} + \eta_{Ohm} + \eta_{Conc}$$

In the pre-reformer unit, 30% of the methane is converted to hydrogen and carbon monoxide before entering the SOFC, thereby minimising SOFC degradation and carbon deposition at the anode [35]. In an SOFC, steam is mixed with methane at a steam-to-carbon ratio of 2.5 to prevent carbon deposition on the anode and facilitate reforming. Table 2 lists the constants involved in SOFC operation.

Table 2. Assumed values of SOFC component parameters [25]

Parameter	Value
Electrolyte resistivity constants	A=.00294, B=10350
Electrolyte thickness	0.004 cm
Cathode Resistivity Constants	A = 0.00811, B = 600
Cathode thickness	0.190 cm
Anode Resistivity Constants	A = 0.00298, B = -1392
Anode thickness	.010 cm
Interconnect resistivity constants	A = 0.1256, B = 4690
Interconnect thickness	0.004 cm
SOFC stack pressure drop	2%
Steam to carbon ratio	2.5
LHV of methane	802000 kJ/kmol
R	8.3143 J mol K
Chemical exergy of methane	830174.37 kJ/kmol
Fuel utilization factor	.85
Oxygen utilization factor	.25

Methane is converted into electrochemically active species via the endothermic Methane Steam Reforming (SR) reaction in the prereformer section.

$$CH_4 + H_2O = CO + 3H_2$$

The endothermic Water Gas Shifting (WGS) reaction within the anode is

$$CO + H_2O = CO_2 + H_2$$

The equilibrium constant is calculated from the partial pressure of the products and reactants.

$$K_{sr} = \frac{p_{CO} p_{H_2}^3}{p_{CH_4} p_{H_2O}}$$

$$K_{wgs} = \frac{p_{CO_2} p_{H_2}}{p_{CO} p_{H_2O}}$$

Temperature-dependent equilibrium constants for reforming reactions have been calculated using.

$$\log K = AT^4 + BT^3 + CT^2 + DT + E$$

The values of the constants are given in Table 3.

Table 3. Equilibrium constants of reforming and shifting reactions [24]

Constants	SR	WGS
A	-2.631 x 10^{-11}	5.47301 x 10^{11}
B	1.24065 x 10^{-7}	2.57479 x 10^{-8}
C	-2.25232 x 10^{-4}	4.63732 x 10^{-8}
D	1.95028 x 10^{-1}	1.32097 x 10^{-2}
E	-6.61395 x 10^{1}	1.32097 x 10^{1}

Three components frame the heat balance equation: Q_{sr} is necessary for SR, Q_{wgs} is necessary for WGS reactions, and Q_{ce} is generated from the exothermic electrochemical reaction. The net heat generated Q within the SOFC stack is

$$Q = Q_{sr} + Q_{wgs} + Q_{ce}$$

The three components are determined from enthalpies, entropies and current density. These calculations are solved through iteration. The SOFC power is then determined from the actual cell voltage (V) and the total current (I) in A, assuming a current density of 0.3 A/cm^2. The oxygen utilisation factor of .25 is suitable for maintaining a sustainable temperature within SOFC components and for adequate air supply to the cathode. The prereformer is modelled with the outlet temperature determined from an enthalpy balance between the inlet streams of methane and steam and the reformate mixture.

3.2.2. Combustion Chamber Modelling

The combustion chamber model assumes complete combustion of all species and accounts for pressure losses. The inlet gas comprises CH_4, H_2, CO, H_2O, CO_2 and excess O_2, which are released from the SOFC, along with fresh methane fuel that can be diverted from the fuel compressor line, undergo the following oxidation reactions

$$CH_4 + 2O_2 = CO_2 + 2H_2O$$

$$H_2 + \frac{1}{2}O_2 = H_2O$$

$$CO + \frac{1}{2}O_2 = CO_2$$

The heat released during the complete combustion of anode exhaust gases is evaluated using the LHV of H_2 (241000 kJ/kmol), CH_4 (802700 kJ/kmol), and CO (283210 kj/kmol). The outlet temperature of the CC exhaust is determined iteratively using an energy balance that accounts for the chemical energy and sensible enthalpy of the inlet streams. Pressure losses are modelled using fixed fractional pressure losses.

3.3. Compressor

The air compressor receives a fixed amount of inlet air comprising 21% Oxygen and 79% nitrogen (on a molar basis). The fuel compressor is fed methane. The temperature-dependent property, i.e., specific heat at constant pressure, was determined using polynomial correlation. The compressor outlet temperature was evaluated using. $\int_{T_1}^{T_2} \frac{C_p}{T}\, dT$.

3.4. Gas Turbine

The working fluid from the SOFC, with different gas molar fractions, is fed into the turbine. The temperature-dependent thermodynamic properties are determined from pressure losses, and turbine output is evaluated using mass- and energy-balanced thermodynamic relations.

3.5. Recuperator & HRSG

The air and fuel recuperators are modelled as counter-flow heat exchangers to preheat the compressed air and methane fuel using the effectiveness-NTU approach. Here, the maximum heat transfer is determined through

$$Q_{max} = C_{min}(T_{hot,inlet} - T_{cold,outlet})$$

With the predefined heat effectiveness value, the actual heat transfer rate Q can be determined from $Q_{actual} = \varepsilon Q_{max}$.

The inlet temperatures of the hot and cold streams determine the outlet temperature of the heat exchangers. The HRSG operates without pinch-point constraints, assuming the maximum possible heat recovery condition. The HRSG comprises an economiser, evaporator and a superheater unit. The enthalpy change of the exhaust gas is the heat gained by the cold fluid (water) during steam generation-Table 4 lists all the efficiencies and effectiveness of the components of the power plants.

Table 4. Assumed values of other component parameters [22]

Parameter	Value
Isentropic efficiency of the turbine	.90
Mechanical efficiency of the turbine	.95
Isentropic efficiency of the air and fuel compressor	.93
Isentropic efficiency of the fuel compressor	.93
Mechanical efficiency of the air and fuel Compressor	.95
Efficiency of the combustion chamber	.98
Inverter efficiency for fuel cell power output	.965
Electrical efficiency of the generator of GT	.98
Effectiveness of the recuperators	.80

3.6. Irreversibilities of the Components

Irreversibility will arise in any actual process, as it is not possible to design a system that can perform all operations reversibly. The effect of Irreversibility is quantified by entropy generation in the steady-state exergy balance across the components.

Chemical exergy for species i in both the inlet and outlet stream is given by

$$\dot{E}^{ch} = \sum_i n_i \, [ex_{ch,i} + RT_0 \ln(X_i)]$$

Physical exergy for species i in both the inlet and outlet stream is given by

$$\dot{E}^{phy} = \sum_i n_i \, [\bar{h}_i(T) - \bar{h}_i(T_0) - T_0(\bar{s}_i^o(T) + (\bar{s}_i^o(T_0) - \bar{R}\ln(\frac{p}{P_0})]$$

The sum of chemical exergy $\dot{E}_{ch}$ and physical exergy$\dot{E}_{ph}$ yields the total exergy.

$$\dot{E} = \dot{E}_{ch} + \dot{E}_{ph}$$

$\dot{I}_{SOFC}$ Is the exergy destruction rate determined from the exergy balance equation as the difference between the total inlet exergy rate? $\dot{E}_{in}$ and the sum of the total outlet exergy rate $\dot{E}_{out}$, and SOFC electrical power output $\dot{W}_{ele}$

$$\dot{I}_{SOFC} = (\dot{E}_{ph,in} + \dot{E}_{ch,in}) - \dot{W}_{SOFC,ele} - (\dot{E}_{ph,out} + \dot{E}_{ch,out})$$

Assuming adiabatic conditions for GT and the absence of any chemical reactions, the irreversibility rate $\dot{I}_{GT}$ is calculated from the difference between the physical exergy rate of the inlet gas stream of the turbine $\dot{E}_{ph,in}$ and the sum of the physical exergy of the turbine exhaust $\dot{E}_{ph,out}$ and the GT shaft work output $\dot{W}_{GT}$.

$$\dot{I}_{GT} = \dot{E}_{ph,in} - (\dot{E}_{ph,out} + \dot{W}_{GT})$$

The combustion chamber irreversibility $\dot{I}_{CC}$ is the difference between the exergy rate of the inlet stream comprising the SOFC exhaust and the additional fuel, and that of the exhaust gases from CC.

$$\dot{I}_{CC} = (\dot{E}_{ph,SOFC} + \dot{E}_{ch,SOFC}) + \dot{E}_{ch,add\ fuel} + \dot{E}_{ph,add\ fuel}) - \dot{E}_{CC,out}$$

In the case of PR, the difference between the exergy rates of the fuel and steam inlet streams and the exergy rate of the reformate leaving PR is

$$\dot{I}_{PR} = (\dot{E}_{fuel,ch} + \dot{E}_{fuel,ph} + \dot{E}_{steam,out} - \dot{E}_{PR,out})$$

For recuperators and HRSGs, the Irreversibility is calculated as the difference between the exergy decrease of the hot stream and the exergy increase of the cold stream.

$$\dot{I}_{HX} = \Delta \dot{E}_{hot} - \Delta\dot{E}_{cold}$$

Assuming adiabatic operation of compressors, Irreversibility is calculated by subtracting outlet flow exergy from the total exergy, equal to shaft work input plus inlet flow exergy.

$$\dot{I}_{comp} = \dot{W}_{shaft,in} + \dot{E}_{in} - \dot{E}_{out}$$

3.7. Thermodynamic Efficiencies

The overall electrical and exergy efficiencies of the SOFC-GT power plant are computed. The hybrid's power output is calculated by summing the individual power outputs of the SOFC and GT, accounting for the inverter and generator efficiency, respectively. Gas turbine power output is determined by subtracting the power required by the fuel and air compressors, which act as parasitic loads, from the turbine shaft power. The isentropic efficiency and mechanical efficiency are considered for both compressors.

$$Net\ AC\ power\ output = \dot{W}_{sofc}.\eta_{inv} + (\dot{W}_{gt} - \dot{W}_{fcomp} - \dot{W}_{acom}).\eta_{gen}$$

4. Simulation Results of the SOFC-GT Plant

Table 5 presents variations in several parameters of the combined SOFC-GT cycle at compression ratios of 8, 10, 12, 14, and 16 under different fuel and air supply conditions. Both the air and fuel compressors operate at the same compression ratio. The readings are generated for 4 different air and additional fuel supply conditions, assuming a constant fuel flow rate of 300 km/hour to the anode, as adopted from the simulation study by Gogoi et al.

The values predicted by the proposed configuration within this range are consistent with those reported by He et al., except for the operating case in which 50% additional fuel is supplied to the CC. Supplying 50% additional fuel reduces efficiency because more of the fuel is converted by combustion than by the more efficient electrochemical conversion in an SOFC. Moreover, increased air supply lowers the SOFC stack temperature, thereby reducing its power output. The power of GT improves marginally, whereas for SOFC it increases only slightly as CPR increases (Figure 3a). For no additional fuel, the AC electrical power outputs of the SOFC and GT at CPR 8 are 28.5 MW and 10.49 MW, respectively, rising to 28.95 MW and 11.97 MW at CPR 16. The contribution of SOFC to total power is significantly higher than that of GT. Increasing CPR results in a higher cell operating pressure, shifting the Nernst potential and causing a gradual, modest increase in SOFC power. The increase in GT power during CPR results from higher inlet pressure, greater enthalpy drop, and higher specific work. However, increasing the additional fuel flow to the CC substantially increases the GT power output. For additional fuel and air supplies of 50 kmol/hr and 4000 kmol/hr, the GT power output increases from 13.56 MW at 8 CPR to 16.5 MW at 16 CPR. GT power further increases to 16.50 MW at 8 CPR and 19.68 MW at 16 CPR, with additional fuel and air supplies of 100 kmol/hr and 4000 kmol/hr, respectively. The highest power is achieved with an additional fuel supply of 150 kmol/hr, raising GT power to 23.46 MW. This is due to the higher combustion temperature, which increases the available work and the exhaust gas mass flow rate. The increase in GT power output, however, is not linear with CPR, because more compression work is extracted from the turbine shaft. However, the SOFC power output decreases modestly with increasing air and additional fuel supply, as increased air flow cools the stack and reduces cell voltage, as evidenced by stack temperature readings that show a decreasing trend with increasing air flow rate at any CPR. Lowering the stack temperature lowers the SOFC cost and degradation rate [36]. In thermodynamic efficiency, both energy and exergy efficiencies increase with increasing CPR (Figure 3). The plant energy and exergy efficiencies increase from 58.34% and 56.36% at 8 CPR to 61.23% and 59.15% at 16 CPR when the additional fuel supply is zero (Figure 3b). Increasing compression ratios improves power output for the same fuel input, thereby raising the electrical power-generation efficiency. The exergy efficiency improvement is due to a reduction in total Irreversibility from 24941 kW at CPR=8 to 23195 kW at CPR=16, indicating a decrease in exergy destruction at the component level. As pressure increases, fuel cell operation approaches reversibility, reducing the exergy loss in the exhaust and thereby lowering entropy generation. However, for the same CPR values, energy efficiency and exergy decrease as the airflow rate and the additional fuel supply increase.

At 16 CPR, the exergy and energy efficiencies decrease from 56.73% and 54.81% to 53.29% and 51.48%, respectively, as the air and additional fuel supply rates increase from 4000 kmol/hr and 50 kmol/hr to 4500 kmol/hr and 100 kmol/hr. The energy and exergy efficiencies further decrease to 50.24 and 48.54, respectively, as the air-supply rate increases to 5000 kmol/hr, with an additional fuel rate of 150 kmol/hr, thereby reducing the SOFC's exergy efficiency due to increased entropy generation and Irreversibility associated with stack cooling. For GT, the additional fuel results in greater chemical exergy destruction and, consequently, greater entropy generation. Therefore, the exergy and energy efficiency decrease despite an increase in net power output. The highest achievable gas turbine inlet temperature with current technologies is 1873 K, as reported in the literature [37-39]. From Table 3, it is observed that at an airflow of 150 kmol/h, the TIT is within the range 1771-1776 K. At this ratio, the plant would generate a maximum of 50.36 MW net AC power, as the GT power is the highest. However, high-temperature SOFCs operate in the 900-1100 K range. Therefore, researchers tend to maintain the TIT below 1500 K to avoid coupling constraints [40, 41]. Additional fuel burned in the CC to increase TIT and improve GT power causes significant exergy loss, as evidenced by the results. A trade-off exists: improving GT power output entails sacrificing the plant's energy and exergy efficiencies due to the destruction of available energy and reduced SOFC output.

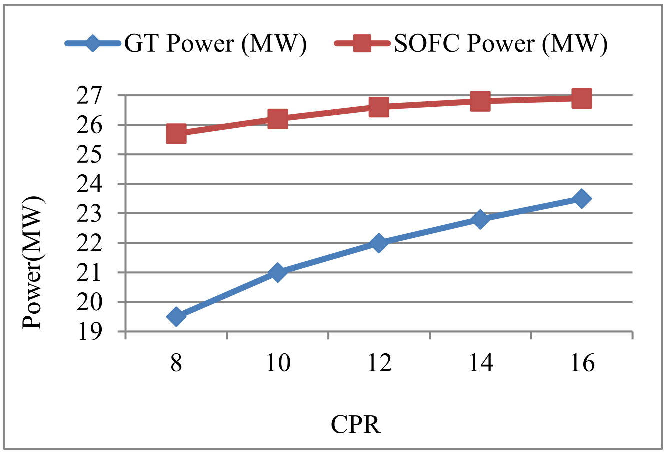

Fig. 3 (a) CPR versus power at 150 kmol/h additional fuel supply

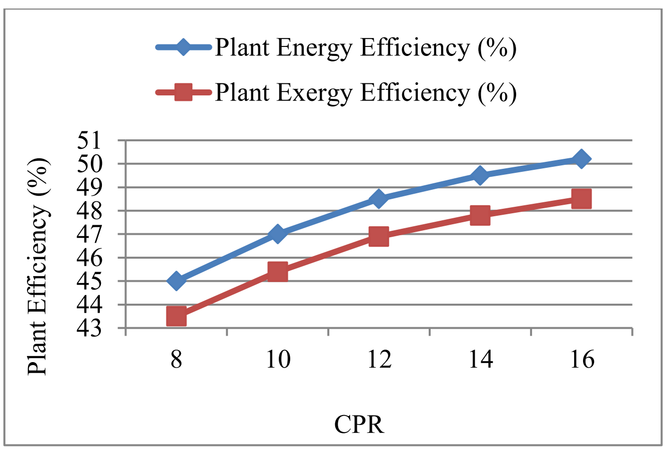

Fig. 3 (b) CPR versus efficiency at 150 kmol/hr additional fuel supply

The HRSG unit produces steam that increases with additional fuel and air supply. Without an additional fuel supply, it produces steam in the range of 6.82-6.88 kg/sec. When the additional fuel of 50 kmol/hr and 100 kmol is supplied, steam generation increases to 8.64-8.80 kg/sec and 10.47-10.81 kg/sec, respectively. The system generates 12.27-12.58 kg/sec when additional fuel is 150 kmol/hr. Increasing supplementary fuel raises GT exhaust temperature, thereby increasing recoverable heat in the HRSG and ultimately increasing steam output.

Figure 3c illustrates the Irreversibility of the components, with significant exergy destruction. The maximum exergy destruction occurs in the SOFC unit, despite being the thermodynamically most efficient component. SOFC converts the fuel's highest chemical exergy in the SOFC-GT power plant.

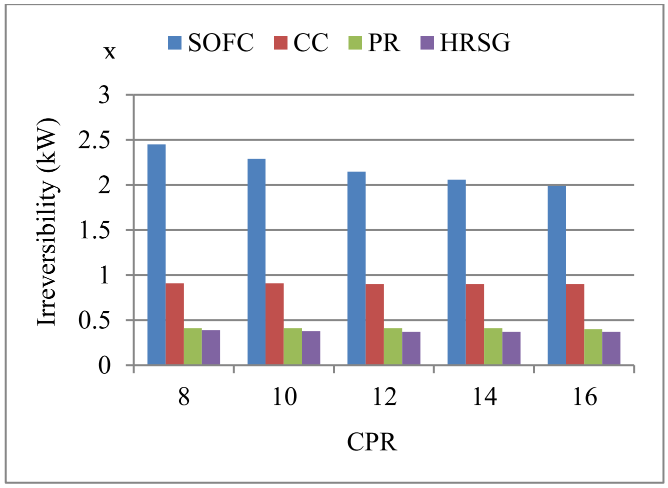

Fig 3 (c) CPR versus Irreversibility at 150 kmol/h additional fuel supply.

Additionally, ohmic losses, activation and concentration losses, and mixing Irreversibility contribute to the SOFC's Irreversibility. The next significant component, where exergy is mostly destroyed, is the combustion chamber, where additional fuel is combusted along with the incoming exhaust stream from the SOFC unit—the chemical exergy conversion of the inlet fuel stream results in substantial chemical exergy destruction inside the CC. Within the HRSG unit, a finite temperature difference between the exhaust gas and steam, particularly during the phase change process, generates entropy. For a prereformer, the non-equilibrium reforming conversion is the primary source of exergy destruction. Additional Irreversibility arises from the endothermic steam methane reforming reaction and from finite-temperature heat transfer during energy supply. The contribution of the remaining components to the total Irreversibility is considerably low [29].

Overall, the increase in CPR has a positive impact on power plant output and efficiency. At an additional fuel supply rate of 150 kmol/hr, increasing CPR from 8 to 16 results in an 11.56% increase in net AC power and a 10.66% decrease in Irreversibility. However, increasing the proportional fuel flow rate improves power and steam production at the cost of plant efficiency. At CPR=16, increasing the additional fuel supply from 0 kmol/hr to 150 kmol/hr, increases the net power output by 23.07% and HRSG steam generation by 78.34% while exergy efficiency decreases by 17.94%.

5. Sensitivity Analysis

Figure 4 shows the plant energy efficiency, exergy efficiency, and total irreversibility results versus the fuel utilisation factor and steam carbon ratio for the first condition, with an air supply rate of 3500 kmol/hr and no additional fuel, at a fixed CPR of 16. The fuel utilisation factor is varied from 0.75 to 0.90 because values below 0.75 would increase combustion in CC and reduce efficiency, while the steam-to-carbon ratio is varied from 2 to 3.5 because values below 2 increase the risk of carbon deposition on the anode [41]. The trendline for FU shows an increase in energy and exergy efficiency up to FU=0.8, remains at 0.85, and then decreases considerably to 57.94% and 55.87% respectively, while total irreversibility increases continuously. Increasing the fuel utilisation factor allows more efficient conversion of methane fuel into electricity within the SOFC, but increasing beyond .85 leaves less fuel for power generation in the GT, leading to a gradual decrease in plant efficiency because the SOFC power gain is insufficient to compensate for the GT power loss. The increase in Irreversibility is due to the depletion of the methane fuel at the anode, driven by enhanced fuel utilisation, and to a decrease in the fuel voltage caused by electrochemical losses and exergy destruction.

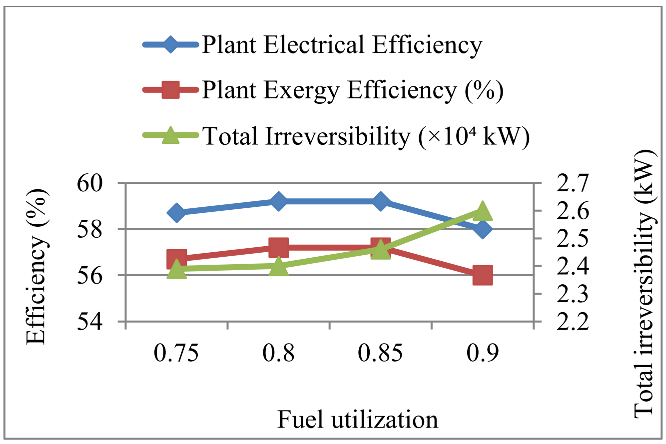

Fig. 4 Efficiency and total Irreversibility vs fuel utilization

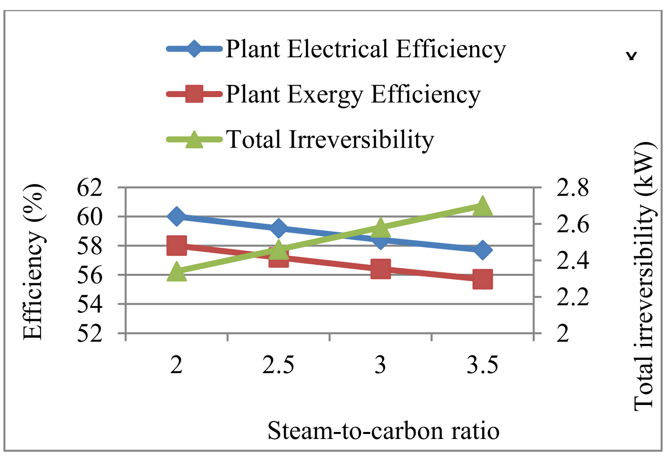

Fig. 5 Efficiency and total Irreversibility vs steam to carbon Ratio

For the steam-to-carbon ratio variation from 2 to 3.5, efficiencies decrease as more steam mixes with the fuel before reaching the anode, and the dilution lowers the cell voltage, reducing efficiency. The Irreversibility increases continuously due to a reduction in the electrochemical potential

6. Conclusion

The simulation-based study presented a thermodynamic analysis of an SOFC-GT hybrid plant integrated with an HRSG to supply process heat for industrial applications. Energy and exergy analyses were conducted for compression ratios of 8-16 by varying the air and additional fuel supply rates.

Results demonstrated that the plant's thermodynamic efficiency increased with increasing CPR. Plant energy efficiency improved from 58.34% at 8 CPR to 61.23% at 16 CPR, while exergy efficiency increased from 56.36% to 59.15% without additional fuel supply.

The efficiency improvement can be attributed to the decrease in total Irreversibility within the system components as system pressure increases. Supplying additional fuel to the CC increases GT power output, thereby increasing plant power output. The GT power output at 16 CPR with no additional fuel is 11.97 MW; it increases to 15.59 MW, 19.68 MW, and 23.46 MW at additional fuel supply rates of 50 kmol/hr, 100 kmol/hr, and 150 kmol/hr, respectively. However, burning additional fuel increases chemical exergy destruction within the CC, thereby reducing the exergetic efficiency of the entire system. Among the components, the maximum exergy was destroyed in the SOFC, despite its being the thermodynamically most efficient, due to electrochemical overpotentials, the Irreversibility of the reforming reaction, and mixing Irreversibility within the SOFC. The second-largest source of exergy destruction is the CC, and the Irreversibility of the prereformer and HRSG arises from finite-temperature heat exchange and reforming reactions. Gas turbine materials limit the Turbine Inlet Temperature (TIT), and keeping TIT below 1500 K is common among researchers due to the relatively high efficiency and flexibility of coupling, compared with the configuration's maximum possible temperature of 1776 K. HRSG steam generation can be varied from 6.67 to 12.88 kg/sec and supplied to industries requiring process steam. Overall, the proposed SOFC-GT configuration integrated with an HRSG shows promise for improving plant performance by generating steam from waste heat. Further thermoeconomic analysis is needed to understand the system's cost-effectiveness better.

Conflicts of Interest

The author declares no conflict of interest.

Funding Statement

The study received no external funding.

References

[1] WMO Confirms 2024 Warmest Year on Record about 1.55°C above Pre-Industrial Level, World Meteorological Organisation, 2025. [Online]. Available: https://wmo.int/news/media-centre/wmo-confirms-2024-warmest-year-record-about-155degc-above-pre-industrial-level

[2] World Energy Outlook 2025, International Energy Agency, pp. 1-519, 2025. [Online]. Available: https://www.iea.org/reports/world-energy-outlook-2025

[3] Electricity Generation, Understand Energy Learning Hub, Stanford University. [Online]. Available: https://understand-energy.stanford.edu/energy-currencies/electricity-generation

[4] More than 60% of Energy used for Electricity Generation is Lost in Conversion, U.S. Energy Information Administration, 2020. [Online]. Available: https://www.eia.gov/todayinenergy/detail.php?id=44436

[5] R. K. Bhargava et al., "Gas Turbine Based Power Cycles – A State-of-the-Art Review," *Challenges of Power Engineering and Environment*, pp. 309-319, 2007. [CrossRef] [Google Scholar] [Publisher Link]

[6] Iliya Krastev Iliev et al., "Theoretical and Experimental Studies of Combined Heat and Power Systems with SOFCs," *Energies*, vol. 16, no. 4, pp. 1-17, 2023. [CrossRef] [Google Scholar] [Publisher Link]

[7] C. T. Cardenas De La Cruz et al., "Modeling of a Novel Atmospheric SOFC/GT Hybrid Process and Comparison with State-of-the-Art SOFC System Concepts," *Fuel Cells*, vol. 20, no. 5, pp. 608-623, 2020. [CrossRef] [Google Scholar] [Publisher Link]

[8] F. Alpegiani et al., "Hybrid Solid Oxide Fuel Cell-Gas Turbines and Triple Combined Cycles Approaching 85% Efficiency," *Applied Thermal Engineering*, vol. 281, no. 1, 2025. [CrossRef] [Google Scholar] [Publisher Link]

[9] Mikhail Granovskii, Ibrahim Dincer, and Marc A. Rosen, "Performance Comparison of Two Combined SOFC–Gas Turbine Systems," *Journal of Power Sources*, vol. 165, no. 1, pp. 307-314, 2007. [CrossRef] [Google Scholar] [Publisher Link]

[10] L. van Biert et al., "A Thermodynamic Comparison of Solid Oxide Fuel Cell-Combined Cycles," *Journal of Power Sources*, vol. 397, pp. 382-396, 2018. [CrossRef] [Google Scholar] [Publisher Link]

[11] Victoria He et al., "Readiness Evaluation of SOFC-MGT Hybrid Systems with Carbon Capture for Distributed Combined Heat and Power," *Energy Conversion and Management*, vol. 278, pp. 1-20, 2023. [CrossRef] [Google Scholar] [Publisher Link]

[12] L.G.J. de Haart, and R. Peters, "Fuel Cells—Solid Oxide Fuel Cells: Internal and External Reformation," *Encyclopedia of Electrochemical Power Sources*, pp. 88-98, 2009. [CrossRef] [Google Scholar] [Publisher Link]

[13] Małgorzata Wójcik, Łukasz Szabłowski, and Olaf Dybiński, "Comparison of Mathematical Models of Steam Methane Reforming Process for the Needs of Fuel Cells," *International Journal of Hydrogen Energy*, vol. 52, pp. 965-982, 2024. [CrossRef] [Google Scholar] [Publisher Link]

[14] Zhen Wu et al., "A Comprehensive Review of Modeling of Solid Oxide Fuel Cells: From Large Systems to Fine Electrodes," *Chemical Reviews*, vol. 125, no. 4, pp. 2184-2268, 2025. [CrossRef] [Google Scholar] [Publisher Link]

[15] Kairat A. Kuterbekov et al., "Classification of Solid Oxide Fuel Cells," *Nanomaterials*, vol. 12, no. 7, pp. 1-22, 2022. [CrossRef] [Google Scholar] [Publisher Link]

[16] Sudhanshu Dwivedi, "Solid Oxide Fuel Cell: Materials for Anode, Cathode and Electrolyte," *International Journal of Hydrogen Energy*, vol. 45, no. 44, pp. 23988-24013, 2020. [CrossRef] [Google Scholar] [Publisher Link]

[17] Dirk Pauschert, "*Study of Equipment Prices in the Power Sector*," World Bank Group, 2009. [Google Scholar] [Publisher Link]

[18] L. S. Langston, *Turbines, Gas*, Reference Module in Earth Systems and Environmental Sciences, 2014. [Publisher Link]

[19] Yoshinori Kobayashi et al., "Extremely High-Efficiency Thermal Power System—Solid Oxide Fuel Cell (SOFC) Triple Combined-Cycle System," *Mitsubishi Heavy Industries Technical Review*, vol. 48, no. 3, pp. 9-15, 2011. [Google Scholar] [Publisher Link]

[20] R.A. Roberts, and J. Brouwer, "Dynamic Simulation of a Pressurized 220 kW Solid Oxide Fuel-Cell-Gas-Turbine Hybrid System: Modeled Performance Compared to Measured Results," *Journal of Fuel Cell Science and Technology*, vol. 3, no. 1, pp. 18-25, 2006. [CrossRef] [Google Scholar] [Publisher Link]

[21] Tae Won Song et al., "Performance Characteristics of a MW-Class SOFC/GT Hybrid System Based on a Commercially Available Gas Turbine," *Journal of Power Sources*, vol. 158, no. 1, pp. 361-367, 2006. [CrossRef] [Google Scholar] [Publisher Link]

[22] A. Cavalli, A. Fernandes, and P.V. Aravind, "Thermodynamic Analysis of an Improved Integrated Biomass Gasifier Solid Oxide Fuel Cell Micro Combined Heat and Power System," *Energy*, vol. 231, pp. 1-14, 2021. [CrossRef] [Google Scholar] [Publisher Link]

[23] Wei Wu, Shin-An Chen, and Ying-Chuan Chiu, "Design and Control of an SOFC/GT Hybrid Power Generation System with Low Carbon Emissions," *Industrial & Engineering Chemistry Research*, vol. 55, no. 5, pp. 1281-1291, 2016. [CrossRef] [Google Scholar] [Publisher Link]

[24] S.H. Chan, H.K. Ho, and Y. Tian, "Modelling of Simple Hybrid Solid Oxide Fuel Cell and Gas Turbine Power Plant," *Journal of Power Sources*, vol. 109, no. 1, pp. 111-120, 2002. [CrossRef] [Google Scholar] [Publisher Link]

[25] S.H. Chan, H.K. Ho, and Y. Tian, "Multi-Level Modeling of SOFC–Gas Turbine Hybrid System," *International Journal of Hydrogen Energy*, vol. 28, no. 8, pp. 889-900, 2003. [CrossRef] [Google Scholar] [Publisher Link]

[26] Brian Tarroja et al., "Parametric Thermodynamic Analysis of a Solid Oxide Fuel Cell Gas Turbine System Design Space," *Journal of Engineering for Gas Turbines and Power*, vol. 132, no. 7, 2010. [CrossRef] [Google Scholar] [Publisher Link]

[27] O. Corigliano, G. De Lorenzo, and P. Fragiacomo, "Techno-Energy-Economic Sensitivity Analysis of Hybrid System Solid Oxide Fuel Cell/Gas Turbine," *AIMS Energy*, vol. 9, no. 5, pp. 934-990, 2021. [CrossRef] [Google Scholar] [Publisher Link]

[28] M. Gandiglio et al., "Thermoeconomic Analysis of Large Solid Oxide Fuel Cell Plants: Atmospheric vs. Pressurized Performance," *Energy*, vol. 55, pp. 142-155, 2013. [CrossRef] [Google Scholar] [Publisher Link]

[29] Y. Haseli, I. Dincer, and G.F. Naterer, "Thermodynamic Analysis of a Combined Gas Turbine Power System with a Solid Oxide Fuel Cell Through Exergy," *Thermochimica Acta*, vol. 480, no. 1–2, pp. 1-9, 2008. [CrossRef] [Google Scholar] [Publisher Link]

[30] Qiao Yuan et al., "Performance Analysis and Optimization of SOFC/GT Hybrid Systems: A Review," *Energies*, vol. 17, no. 5, pp. 1-22, 2024. [CrossRef] [Google Scholar] [Publisher Link]

[31] U.S. Department of Energy, "*Steam System Opportunity Assessment for the Pulp and Paper, Chemical Manufacturing, and Petroleum Refining Industries: Main Report*," Office of Energy Efficiency and Renewable Energy, pp. 1-102, 2002. [Google Scholar] [Publisher Link]

[32] Catalog of CHP Technologies: Section 3 – Technology Characterization – Combustion Turbines, Combined Heat and Power Partnership, U.S. Environmental Protection Agency, pp. 1-22, 2015. [Online]. Available: https://www.epa.gov/sites/default/files/2015-07/documents/catalog_of_chp_technologies_section_3._technology_characterization_-_combustion_turbines.pdf

[33] Maike Johnson, and Michael Fiss, "Superheated Steam Production from a Large-Scale Latent Heat Storage System within a Cogeneration Plant," *Communications Engineering*, vol. 2, pp. 1-10, 2023. [CrossRef] [Google Scholar] [Publisher Link]

[34] T.K. Gogoi, P. Sarmah, and D. Deb Nath, "Energy and Exergy Based Performance Analyses of a Solid Oxide Fuel Cell Integrated Combined Cycle Power Plant," *Energy Conversion and Management*, vol. 86, pp. 507-519, 2014. [CrossRef] [Google Scholar] [Publisher Link]

[35] Quanrong Fu et al., "Performance Study of Solid Oxide Fuel Cell with Ni-Foam Indirect Internal Reformer: Intrinsic Reforming Kinetics and Temperature Uniformity," *Chemical Engineering Journal*, vol. 457, 2023. [CrossRef] [Google Scholar] [Publisher Link]

[36] Xin Gu et al., "Elevating Gas Turbine System Efficiency by Integration with Super-High-Temperature Solid Oxide Fuel Cells," *The Innovation Energy*, vol. 2, no. 3, pp. 1-10, 2025. [CrossRef] [Google Scholar] [Publisher Link]

[37] Janusz Kotowicz, Mateusz Brzęczek, and Marcin Job, "The Thermodynamic and Economic Characteristics of the Modern Combined Cycle Power Plant with Gas Turbine Steam Cooling," *Energy*, vol. 164, pp. 359-3476, 2018. [CrossRef] [Google Scholar] [Publisher Link]

[38] Janusz Kotowicz, and Mateusz Brzęczek, "Analysis of Increasing Efficiency of Modern Combined Cycle Power Plant: A Case Studies," *Energy*, vol. 153, pp. 90-99, 2018. [CrossRef] [Google Scholar] [Publisher Link]

[39] Satoshi Hada et al., "High-Efficiency Gas Turbine Development Applying 1600°C Class 'J' Technology," *Mitsubishi Heavy Industries Technical Review*, vol. 52, no. 2, pp. 2-9, 2015. [Google Scholar] [Publisher Link]

[40] Parisa Kazemiani-Najafabadi, and Ehsan Amiri Rad, "Introducing an Optimum Gas Turbine Inlet Temperature (TIT) based on a 4E Analysis: A Case Study of Northeastern Iran," *Journal of Thermal Analysis and Calorimetry*, vol. 146, no. 1, pp. 403-413, 2021. [CrossRef] [Google Scholar] [Publisher Link]

[41] Denver F. Cheddie, "Integration of a Solid Oxide Fuel Cell into a 10 MW Gas Turbine Power Plant," *Energies*, vol. 3, no. 4, pp. 754-769, 2010. [CrossRef] [Google Scholar] [Publisher Link]

[42] Alexandros Arsalis, "Thermoeconomic Modeling and Parametric Study of Hybrid SOFC–Gas Turbine–Steam Turbine Power Plants Ranging from 1.5 to 10 MWe," *Journal of Power Sources*, vol. 181, no. 2, pp. 313-326, 2008. [CrossRef] [Google Scholar] [Publisher Link]

Appendix

Table 5. System performance at different CPR for varying air and fuel supply

Air and fuel supply (kmol/hr)	CPR	SOFC Power (MW)	GT Power (MW)	Net AC power (MW)	Stack temperature (K)	Plant electrical efficiency (%)	Plant exergy efficiency (%)	TIT(K)	Total Irreversibility (kW)	Steam generated (kg/sec)
N_{fuel} = 300 N_{air}= 3500 $N_{addlfuel}$ = 0	8	28.5	10.49	38.99	1010	58.34	56.36	1406.73	24941	6.88
	10	28.7	11.05	39.75	1006	59.48	57.46	1403.32	24245	6.83
	12	28.84	11.46	40.3	1003	60.3	58.26	1401.22	23742	6.82
	14	28.88	11.78	40.66	1000	60.83	58.77	1399.44	23439	6.83
	16	28.95	11.97	40.92	998	61.23	59.15	1398.95	23195	6.88
N_{fuel} = 300 N_{air} = 4000 $N_{addlfuel}$ = 50	8	27.95	13.56	41.52	1004	53.25	51.44	1555.79	31923	8.80
	10	28.24	14.49	42.73	1001	54.8	52.94	1554.06	30821	8.69
	12	28.37	15.14	43.51	998	55.8	53.9	1552.57	30110	8.64
	14	28.49	15.57	44.06	996	56.51	54.59	1552.24	29574	8.65
	16	28.65	15.59	44.23	995	56.73	54.81	1553	29262	8.74
N_{fuel} = 300 N_{air} = 4500 $N_{addlfuel}$ = 100	8	26.98	16.50	43.48	994	48.80	47.14	1673.8	39435	10.71
	10	27.35	17.73	45.09	992	50.59	48.88	1673.6	37956	10.55
	12	27.67	18.59	46.26	991	51.91	50.15	1674.4	36834	10.49
	14	27.77	19.21	46.99	989	52.73	50.94	1674.6	36140	10.47
	16	27.81	19.68	47.49	987	53.29	51.48	1675.07	35648	10.48
N_{fuel} = 300 N_{air} = 5000 $N_{addlfuel}$ = 150	8	25.68	19.46	45.14	982	45.03	43.50	1770	47284	12.58
	10	26.16	20.96	47.12	981	47	45.4	1771.27	45421	12.39
	12	26.58	22.04	48.62	981	48.5	46.86	1773.41	43961	12.30
	14	26.78	22.81	49.59	980	49.63	47.78	1774.92	43011	12.27
	16	26.9	23.46	50.36	979	50.24	48.54	1776.63	42243	12.27